1550 nm with U-band Raman gains and noise figures (NF), as shown in Fig. 2*a*. The peak Raman small signal gain was 31.6 dB at 1666.4 nm with a corresponding noise figure of 5.3 dB when 1.66 W of post circulator pump power was coupled into the gain fibre.

Using the tuneable Raman fibre laser as pump, wavelength tuneable gain in the L-band was obtained as shown in Fig. 2*b*. The peak Raman gain was 8.7 dB at 1623 nm with a noise figure of 6 dB, for a pump centred at 1515 nm with post circulator power of 420 mW.

Combining the two pump units via a fibre coupler optimised for the lower power, short wavelength pump at 1515 nm gave a flattened gain profile as shown in Fig. 3. Here the EDFA pump was run at full power to compensate the coupler loss, though a reduction would be possible with seeding of the EDFA at a wavelength corresponding to one of the transmission peaks in the coupler. The power coupled into the Raman gain fibre was 365 and 425 mW for the 1515 nm and EDFA pump units, respectively.

The noise figure of the dual pumped amplifier was around 6 dB, with peak Raman gains of 11.5 and 11.4 dB at wavelengths of 1636 and 1666 nm, respectively. The amplifier had a bandwidth of over 50 nm with a gain flatness of < 1.5 dB. Four-wave mixing (FWM) of the two pump wavelengths in the DSF gave a Stokes line at 1600 nm, which would be detrimental to the performance of a transmission system using that region, but this can be reduced with the use of a fibre with higher dispersion around the pump wavelengths. Further improvements in the gain are envisaged with the use of a Raman pump unit optimised for higher output power at 1515 nm than that demonstrated here. This would be possible by replacing the tuneable ring laser with a specifically designed cascade stage. Additionally, a micro-optic based coupler would offer improved multiplexing of the spectrally narrow short wavelength pump and broadband erbium ASE signal.

Conclusions: A U-band EDFA pumped Raman amplifier has been demonstrated with a peak gain of 33 dBm. Simple sources have been developed to probe the gain and noise figure operation over the spectral region 1600–1670 nm. A dual-pumped, single stage amplifier with flattened gain covering the long wavelength region of the L-band and the whole U-band has been characterised 1600–1670 nm. Gain ripple was < 1.5 dB over the spectral range of the U-band with a low noise figure of around 6 dB. We will report at a later date on fibre optimisation and multiple stage configurations of these amplifiers, which should find application in extending the operational bandwidth of future systems.

26 April 2001
Electronics Letters Online No: 20010595
DOI: 10.1049/el:20010595

P.C. Reeves-Hall, D.A. Chestnut, C.J.S. De Matos and J.R. Taylor (*Femtosecond Optics Group, Department of Physics, Imperial College, London SW7 2BW, United Kingdom*)

E-mail: pc.reeveshall@ic.ac.uk

References

1 DAVIDSON, C.R., CHEN, C.J., NISSOV, M., PILIPETSKII, A., RAMANUJAM, N., KIDORF, H.D., PEDERSEN, B., MILLS, M.A., LIN, C., HAYEE, M.I., CAI, J.X., PUC, A.B., CORBETT, P.C., MENGES, R., LI, H., ELYAMANI, A., RIVERS, C., and BERGANO, N.S.: '1800 Gb/s transmission of one hundred and eighty 10 Gb/s WDM channels over 7000 km using the full EDFA C-band'. Optical Fiber Communication Conf., Tech. Dig. Postconference Edn. Trends in Optics and Photonics, 2000, Vol. 37, (4), pp. 242–244

2 STOLEN, R.H., IPPEN, E.P., and TYNES, A.R.: 'Raman oscillation in glass optical waveguide', *Appl. Phys. Lett.*, 1972, **20**, pp. 62–64

3 STOLEN, R.H., and IPPEN, E.P.: 'Raman gain in glass optical waveguides', *Appl. Phys. Lett.*, 1973, **22**, pp. 276–278

4 MASUDA, H., KAWAI, S., SUZUKI, K.-I., and AIDA, K.: '1.65-μm band fibre Raman amplifier pumped by wavelength-tunable broad-linewidth light source'. 24th European Conf. Optical Communication, 1998, Vol. 3, pp. 139–141

5 REEVES-HALL, P.C., and TAYLOR, J.R.: 'Wavelength tunable CW Raman fibre ring laser operating at 1486–1551 nm', *Electron. Lett.*, 2001, **37**, pp. 491–492

Extracting PMD statistics from single emulated fibre sample

A. Vannucci and A. Bononi

To obtain reliable PMD statistics from frequency-swept measurements of emulated fibres, criteria are provided to relate the measurement bandwidth to the fibre mean differential group delay and the number of frequency samples.

Introduction: Polarisation mode dispersion (PMD) effects, such as the differential group delay (DGD), are believed to be ergodic stochastic processes in the frequency domain, thus making it possible to evaluate ensemble averages and distributions over frequency (frequency-swept measurements) as well as over fibre samples (sample-swept measurements) [1, 2]. When frequency-swept measurements are performed, a careless choice of the measurement bandwidth with respect to the fibre parameters can result in serious mismatches with theoretical results [2]. If a fibre is modelled by a concatenation of polarisation maintaining fibre (PMF) sections, as in software simulation or in a laboratory emulator, the number of sections determines the statistical significance of the measurements [3]. We wish to provide a criterion to establish the measurement bandwidth and the number of sections needed to obtain reliable statistics, once the desired number of measurement points and the average DGD are given. Although we will illustrate the implications of such choices on the estimation of the DGD distribution, the given criteria can be applied to the statistical measurement of other PMD effects.

Choice of measurement bandwidth: The maximum number of significant (i.e. almost uncorrelated) frequency samples obtained from each fibre sample is limited by the correlation bandwidth of the elements of the Jones matrix, which is known to be $\Delta B_U = 4/(\langle\Delta\tau\rangle\pi\sqrt{3})$ Hz [4], for long fibres. Assuming that the DGD is measured with the Jones matrix method [5], N_ω DGD values are obtained from the measurement of the Jones matrix at $N_\omega + 1$ equally spaced frequency values in a bandwidth ΔB. For the estimation of distributions of the DGD and related quantities from one fibre sample, two conditions must be met: the measurement bandwidth must be much larger than the correlation bandwidth, to reduce the statistical dependence of the data set, and the frequency step must be sufficiently smaller than the correlation bandwidth, to avoid an inaccurate approximation of the derivative $\mathbf{U}'(\omega)$. These conditions can be compactly expressed as

$$\Delta B_U \ll \Delta B < N_\omega \Delta B_U \tag{1}$$

The best heuristic value for ΔB is found to be between one-tenth and one-quarter of the upper limit: beyond such value, the DGD distribution tends to be more peaked than a Maxwellian distribution. As a rule of thumb, we can set

$$\Delta B = \frac{N_\omega}{4\sqrt{3}}\Delta B_U = \frac{N_\omega}{3\pi\langle\Delta\tau\rangle} \tag{2}$$

DGD distribution for a single simulated fibre: A birefringent fibre can be simulated by concatenating N independent PMF plates [3]. The Jones matrix $\mathbf{U}_n(\omega)$ of each nth plate is characterised by Stokes eigenvectors uniformly distributed on the equator of the Poincaré sphere (since silica fibres are linearly birefringent) and by eigenvalues $\exp(\pm i\Delta\phi_n(\omega)/2)$ where the retardation angle is $\Delta\phi_n(\omega) = \Delta\phi_{n0} + \Delta\phi_{n1}\omega$. The term $\Delta\phi_{n0}$ is assumed uniform on $[0; 2\pi]$ in [3], while it is neglected in [6]; $\Delta\phi_{n1}$ has a Gaussian distribution with standard deviation equal to 20% of its mean value. The RMS DGD of the fibre can be chosen by resorting to the Gisin–Pelleaux recursion [6]: $\langle\Delta\tau^2\rangle = N\langle\Delta\phi_{n1}^2\rangle$, where $\langle\cdot\rangle$ denotes expectation. Fig. 1*a* shows the DGD distribution obtained from 1000 frequency-swept measurements of a single $N = 15$ plates simulated fibre sample, with a nominal RMS DGD of 10 ps. The broken line shows a Maxwellian fitting curve. The correlation bandwidth is 73 GHz in this case, corresponding to about 0.6 nm at a reference wavelength of 1555 nm. We chose a measurement bandwidth of 60 nm, a little less than the value 85 nm obtained from eqn. 2. Strictly speaking, the result given for ΔB_U only applies to 'long' fibres, i.e. those composed of a large number of plates. However, eqn. 2 can serve as a guideline even when N is not too large, as in

the present case. In Fig. 1*b* the measurement bandwidth is reduced to only 4 nm, for the same fibre realisation. Such wavelength range is close to the correlation bandwidth, and the distribution so obtained is far from a Maxwellian fit. A similar problem occurs in [2], where a 15 section emulator, with mean DGD of about 50 ps, is swept over just 1 nm. Of course, repeating the measurements on more fibre samples improves the accuracy of the estimated distribution. If a careless choice of ΔB is made, as in Fig. 1*b*, several hundred fibre samples are needed to obtain an estimation of the distribution comparable to that of Fig. 1*a*.

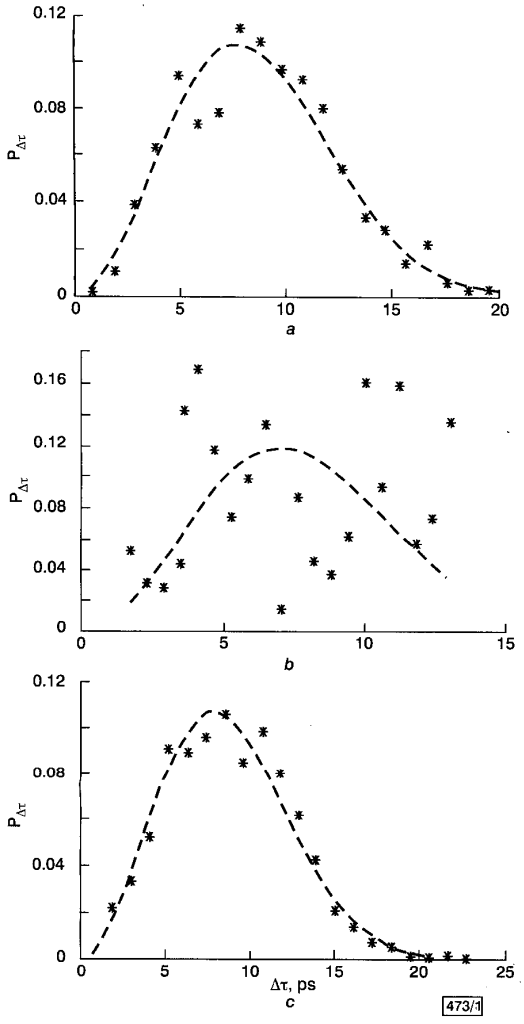

Fig. 1 *DGD distribution obtained from simulation of single fibre*

a 15 plates, measurement bandwidth 60 nm
b 15 plates, measurement bandwidth 4 nm
c 6000 plates, measurement bandwidth 60 nm
* frequency-swept measurements
– – – Maxwell fitting

Fibre periodicities in the retarded plate model: If, in the retarded plate model described above, $\Delta\phi_{n1}$ is the same for every plate, the global Jones matrix $\mathbf{U}(\omega)$, along with any quantity measured from it, such as $\Delta\tau(\omega)$, has the period of the eigenvalues of $\mathbf{U}_n(\omega)$. The number of periods observed in a bandwidth of ΔB is

$$n_p = \Delta B \Delta\phi_{n1} = \Delta B \langle\Delta\tau\rangle \sqrt{\frac{3\pi}{8N}} \qquad (3)$$

and we must ensure that $n_p < 1$ for meaningful frequency-swept measurements. Such condition is in substantial agreement with eqn. 26 in [7]. Clearly, frequency periodicities are not an issue when sample-swept measurements are performed and only one measurement is taken from each fibre sample. However, such approach requires many fibre samples, and is thus time-consuming in simulations and extremely impractical in fibre emulation. The adoption of a random $\Delta\phi_{n1}$, with the described Gaussian distribution, is reported in [3] to overcome the problem of periodicity: we relied on such choice in the previous Section. However, we found that this countermeasure is not effective with a small number of plates N. Simulations with only $N = 3$ plates show clearly that the periodicities induced by a fixed $\Delta\phi_{n1}$ are only perturbed and turned into 'quasi-periodicities' when $\Delta\phi_{n1}$ is random, as above. In fact, varying N, the estimated distribution of Fig. 1*a* is observed to vary its accuracy accordingly: for $N < 10$ it is far from Maxwellian , while for $N \gg 15$ its accuracy increases, at the expense of an increased complexity of the simulated model [2]. We will show that reliable distributions for the DGD can be obtained even in the presence of a fixed $\Delta\phi_{n1}$, provided that the number of plates and the measurement bandwidth are suitably chosen.

DGD distribution with fixed $\Delta\phi_{n1}$*:* Computing the DGD distribution as in Fig. 1*a*, with a fixed $\Delta\phi_{n1}$, a totally unacceptable distribution is obtained, since ΔB includes $n_p = 20$ periods, from eqn. 3, resulting in a redundant data set. The only way to obtain N_ω significant measurements is to increase the number of plates N, so that $n_p < 1$. If ΔB is chosen as in eqn. 2, then from eqn. 3 we see that N depends on ΔB^2, hence on N_ω^2: Thus, if N_ω is large, N becomes prohibitively large. An alternative strategy, instead of using eqn. 2, is to choose ΔB equal to n_c times the correlation bandwidth, with $1 \ll n_c < N_\omega/(4\sqrt{3})$, still satisfying eqn. 2: the condition $n_p < 1$ becomes

$$N > \frac{2n_c^2}{\pi} \qquad (4)$$

In Fig. 1*c* we report the DGD distribution obtained from 1000 frequency-swept measurements of a single simulated fibre sample with fixed $\Delta\phi_{n1}$. The fibre consists of $N = 6000$ plates, resulting from eqn. 4 for n_c equal to about 100. The RMS DGD is 10 ps, as in the previous figures, hence the measurement bandwidth is $n_c\Delta B_U = 60$ nm, as in Fig. 1*a*. Values of n_c much smaller than 100 yield inaccurate estimations of the DGD distribution; hence, from eqn. 4, N always needs to be extremely large to ensure reliable statistics when $\Delta\phi_{n1}$ is fixed. Although such a large number of plates is impractical, and a random $\Delta\phi_{n1}$ is always advisable in fibre simulation and emulation, the good match between measured data and the Maxwellian fitting curve in Fig. 1*c* proves that, at least in principle, reliable statistics can be obtained from a single fibre sample, even when $\Delta\phi_{n1}$ is fixed. Another important implication of this result is that the origin of the Maxwellian distribution of the DGD is not dictated by the local fluctuations of the coefficient $\Delta\phi_{n1}$ but rather by a short correlation length, i.e. large N.

Conclusion: If the DGD, or any other birefringence effect, has to be statistically characterised through fibre simulation/emulation, a single fibre sample can be used to perform frequency-swept measurements with an acceptable degree of accuracy, provided we properly select the frequency bandwidth ΔB (eqn. 2) if $\Delta\phi_{n1}$ is random, or both ΔB and the number of plates (eqn. 4) if $\Delta\phi_{n1}$ is fixed.

8 May 2001
Electronics Letters Online No: 20010627
DOI: 10.1049/el:20010627

A. Vannucci and A. Bononi (*Dipartimento di Ingegneria dell'Informazione, Università di Parma, 43100 Parma, Italy*)

E-mail: vannucci@tlc.unipr.it

References

1 GISIN, N.: 'Solutions of the dynamical equation for polarization dispersion', *Opt. Commun.*, 1991, **86**, pp. 371–373

2 LIMA, I.T., KHOSRAVANI, R., EBRAHIMI, P., IBRAGIMOV, E., WILLNER, A.E., and MENYUK, C.R.: 'Polarization mode dispersion emulator'. Proc. OFC 2000, 2000, Paper ThB4, pp. 31–33

3 DAL FORNO, A.O., PARADISI, A., PASSY, R., and VON DER WEID, J.P.: 'Experimental and theoretical modeling of polarization-mode dispersion in single-mode fibers', *IEEE Photonics Technol. Lett.*, 2000, **12**, pp. 296–298

4 BONONI, A., and VANNUCCI, A.: 'Statistics of the Jones matrix of fibers affected by polarization mode dispersion', accepted for publication in *Opt. Lett.*, 2001, **26**, (10)

5 HEFFNER, B.L.: 'Automated measurement of polarization mode dispersion using Jones matrix eigenanalysis', *IEEE Photonics Technol. Lett.*, 1992, **4**, (9), pp. 1066–1069
6 GISIN, N., and PELLEAUX, J.P.: 'Polarization mode dispersion: time versus frequency domains', *Opt. Commun.*, 1992, **89**, pp. 316–323
7 LI, Y., EYAL, A., and YARIV, A.: 'Higher order error of discrete fiber model and asymptotic bound on multistaged PMD compensation', *IEEE J. Lightwave Technol.*, 2000, **18**, (9), pp. 1205–1213

Impulsive pump depletion in saturated Raman amplifiers

A. Bononi, M. Papararo and A. Vannucci

The analytical results available for counter-propagating pump distributed Raman amplifiers in the undepleted pump approximation are shown to be easily extended to the signal-saturated case by using effective values of both input pump and signals.

Introduction: The quantities of most interest in counter-propagating pump distributed Raman amplifiers are easily obtained in closed form in the unsaturated regime, in which the pump is not appreciably depleted by the signals [1 – 3]. In this Letter we show that such results are valid in signal-saturated amplifiers, provided a smaller, effective input pump value, and pre-emphasised effective input signal values are used. A single transcendental equation must be solved to find the pump reduction factor. Consider the case of N channels of average power S_{j0}, $j = 1, ..., N$, injected in a fibre L kilometres long, pumped from the output by a single pump of power P_0, with signal attenuation α_s and pump attenuation α_p. Neglecting noise, Rayleigh scattered signal power, and signal-signal Raman crosstalk, the implicit solution of the propagation equations in the $+z$ direction for pump and signals is:

$$P(z) = P_0 e^{-\Gamma(z)} e^{\alpha_p (z-L)} \tag{1}$$

$$S_j(z) = S_{j0} e^{\left(-\alpha_s z + \gamma_{pj} \int_0^z P(z')dz'\right)} \tag{2}$$

for $j = 1, ..., N$, where $\gamma_{pj} > 0$ is the modal Raman gain factor [$W^{-1}km^{-1}$] from the pump at λ_p to a signal at λ_j, $\hat{\gamma}_{pj} \triangleq \gamma_{pj}(\lambda_j/\lambda_p)$, and where

$$\Gamma(z) \triangleq \sum_{j=1}^{N} \hat{\gamma}_{pj} K_j(z) S_j(L) \tag{3}$$

is the pump depletion factor, and

$$K_j(z) \triangleq \int_z^L \frac{S_j(z')}{S_j(L)} dz' \tag{4}$$

for $j = 1, ..., N$. To obtain an explicit form of eqns. 1 and 2, some approximations are necessary.

Impulsive pump depletion: The impulsive pump depletion approximation relies on the signals mostly depleting the pump within a very short distance from the link output, where the pump is injected. Hence $P(z)$ at those z values where the pump power is significant for amplification can be accurately predicted by concentrating the depletion at the very end of the link. This amounts to approximating $S_j(z')$ in eqn. 4 as a Dirac impulse placed at $z' = L$, so that K_j is z-independent, and so is Γ. Hence we can define the effective injected pump power as

$$P_0^{eff}(\Gamma) = P_0 e^{-\Gamma} \tag{5}$$

so that the explicit form of eqns. 1 and 2 is:

$$P(z) = P_0^{eff}(\Gamma) e^{\alpha_p (z-L)} \tag{6}$$

$$S_j(z) = S_{j0} e^{\left[-\alpha_s z + Q_j(\Gamma) e^{-\alpha_p L}(e^{\alpha_p z} - 1)\right]} \tag{7}$$

where $Q_j(\Gamma) \triangleq \gamma_{pj} P_0^{eff}(\Gamma)/\alpha_p$; i.e. the same equations as in the undepleted pump approximation are obtained [3], provided that we use the effective pump power P_0^{eff} instead of P_0. An approximate expression for the unknowns K_j can now be obtained considering that, to get an accurate expression for the signal power in eqn. 2, a good approximation of the pump $P(z)$ in eqn. 1 is needed only for z, being not too far from the output, where the pump is large and thus Raman amplification of the signals is significant. Hence using eqn. 7 in eqn. 4 we obtain

$$\begin{aligned} K_j &= \int_z^L e^{\left[-\alpha_s (z'-L) + Q_j \left(e^{\alpha_p (z'-L)} - 1\right)\right]} dz' \\ &\simeq \int_0^L e^{\left[(\alpha_p Q_j - \alpha_s)(z'-L)\right]} dz' \\ &= \frac{1 - e^{-(\alpha_p Q_j - \alpha_s)L}}{\alpha_p Q_j - \alpha_s} \end{aligned} \tag{8}$$

where in the second line we linearised the exponential term $e^{\alpha_p (z'-L)}$ of the first line. Using such $K_j(\Gamma)$ and eqn. 7 in eqn. 3 gives a transcendental equation from which the pump depletion factor Γ can be obtained:

$$\Gamma = \sum_{j=1}^{N} \hat{\gamma}_{pj} K_j(\Gamma) S_{j0} e^{\left[-\alpha_s L + Q_j(\Gamma)(1 - e^{-\alpha_p L})\right]} \tag{9}$$

This procedure gives accurate results for the output signal powers if the injected signals have low power, so that signal-signal Raman crosstalk is negligible. Otherwise there is a simple trick to account for such crosstalk. It is sufficient to (i) evaluate the power tilt that would be induced by signal-signal Raman crosstalk in the unpumped fibre [4]:

$$T_j \triangleq \frac{S_T}{\sum_{k=1}^{N} S_{k0} \exp\left\{-\gamma_{kj} S_T \frac{1 - e^{-\alpha_s L}}{\alpha_s}\right\}} \tag{10}$$

where $S_T = \Sigma_{j=1}^{N} S_{j0}$ is the total launched signal power, and the modal Raman gain γ_{kj} is positive for $\lambda_k > \lambda_j$, and negative otherwise; (ii) then use the effective input signal power $S_{j0}^{eff} = T_j S_{j0}$ instead of S_{j0} in eqns. 7 and 9.

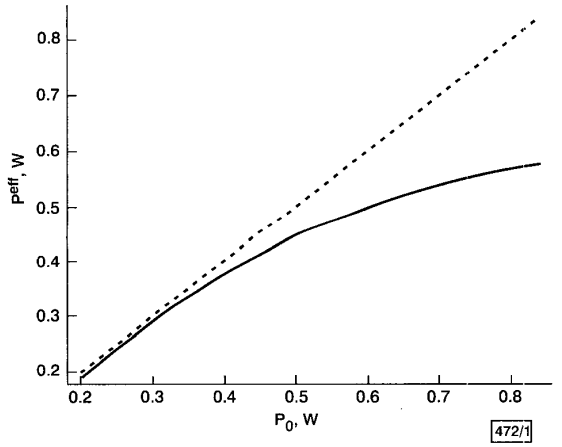

Fig. 1 *Effective pump power against input pump power*

Numerical results: To illustrate the procedure, consider a link of L = 150 km of NZDSF$^+$ fibre, with α_s = 0.205 dB/km, α_p = 0.265 dB/km, with peak Raman gain 0.740 $W^{-1}km^{-1}$. N = 50 channels with spacing 0.8 nm, from 1513.8 to 1553 nm, all with power S_{j0} = 6.3 mW (8 dBm), are launched at the input, with a counter-propagating pump at λ_p = 1438 nm. Fig. 1 shows the effective pump power eqn. 5 against input pump power P_0. It is seen that at small pump values $P_0^{eff} \cong P_0$, while at large pump values the effective pump tends to saturate. Fig. 2 shows the power evolution along the line of both pump and three selected signals, those at channels 20, 30 and 40. Solid lines represent the exact powers, evaluated by solving the complete propagation equation. Dotted lines refer to the values obtained in the simple undepleted pump approximation, i.e. assuming $P(z) = P_0 e^{\alpha_p (z-L)}$. Clearly, such approximation is unrealistic at such signal values. Dashed line values represent our impulsive pump approximation, which makes use of the effective pump and signal powers. It can be seen that using the effective input signal powers S_{j0}^{eff}, as per eqn. 10, has the effect of treating